Synthesis and In Vitro Studies of a Gd(DOTA)–Porphyrin Conjugate for Combined MRI and Photodynamic Treatment

Sébastien Jenni, Celia Bonnet, Frédéric Bolze, Agnes A. Pallier, Angélique Sour, Éva Tóth, Barbara Ventura, Valérie Heitz

Synthesis and in vitro studies of a Gd(DOTA)-porphyrin conjugate for combined MRI and photodynamic treatment

Sébastien Jenni[†], Frédéric Bolze[‡], Célia S. Bonnet[⊥], Agnès Pallier, Angélique Sour[†], Éva Tóth[*⊥], Barbara Ventura[*‖] and Valérie Heitz[*†]*

† Laboratoire de Synthèse des Assemblages Moléculaires Multifonctionnels, Institut de Chimie de Strasbourg, CNRS/UMR 7177, Université de Strasbourg, 4 rue Blaise Pascal, 67000 Strasbourg, France

‡ CAMB, UMR 7199, Unistra/CNRS, Faculté de Pharmacie, Université de Strasbourg, 74 route du Rhin, 67401 Illkirch, France

⊥ Centre de Biophysique Moléculaire, CNRS UPR 4301, Université d'Orléans, rue Charles Sadron, CS 80054, 45071 Orléans Cedex 2, France

‖ Istituto ISOF-CNR, via P. Gobetti 101, 40129 Bologna, Italy

ABSTRACT

With the aim of developing new molecular theranostic agents, a π-extended Zn(II) porphyrin as photosentizer for photodynamic therapy (PDT) linked to two GdDOTA-type complexes for magnetic resonance imaging (MRI) detection was synthesized. The relaxivity studies revealed a much higher relaxivity value per Gd ion for this medium size molecule (19.32 $mM^{-1}s^{-1}$ at 20 MHz and 298 K) compared to clinical contrast agents, a value which strongly increases in presence of bovine serum albumin reaching 25.22 $mM^{-1}s^{-1}$. Moreover, the photophysical studies showed the strong ability of the molecule to absorb light in the deep red (670 nm, $\varepsilon \approx 60\,000\ M^{-1}\ cm^{-1}$) and in the near infra-red following two-photon excitation (920 nm, $\sigma_2 \approx 650$ GM). The conjugate is also able to generate singlet oxygen, with a quantum yield of 0.58 in DMSO. Promising results were obtained in cellular studies, demonstrating that the conjugate is internalized in HeLa cells at micromolar concentration and leads to 70% of cell death following 30 mn irradiation at 660 nm. These results confirm the potential of the designed molecule as an imaging and therapeutic agent.

INTRODUCTION

Theranostics is an emerging approach in medicine which targets the development of personalized treatments based on early stage diagnosis and optimized medical protocols provided by the combination of imaging and therapeutic agents into a single molecular device.[1-3] Theranostic agents have the promise of making diagnosis more accurate, informing about the localization of the drug and providing more efficient treatment at lower dose by monitoring the outcome of the treatment at every stage. In this context, combining photodynamic therapy (PDT) and magnetic resonance imaging (MRI) is appealing, due to the numerous merits of both modalities and to synergetic effects that can be obtained *via* their association.[4]

Photodynamic therapy (PDT) is a non-invasive medical treatment approved for cancer and various non-malignant diseases.[5] It requires a non-toxic photosensitizer (PS) that, once accumulated at the tumor site, is excited by light to trigger photochemical reactions. Thus, in its excited triplet state the PS reacts with surrounding oxygen by energy transfer or with biological substrates by electron transfer. The resulting, highly cytotoxic singlet oxygen and reactive oxygen species induce cell death, tissue and microvasculature destruction. Moreover, PDT was also shown to induce inflammatory and anti-tumor immunity.[6-8] PDT key advantages are the inherent spatiotemporal control of the treatment provided by light excitation at the tumor site, which limits the damage to normal tissue, its repeatability without cumulative toxicity, and the absence of resistance developed to the treatment due to non-specific mechanisms involved in cell death. PDT gradually gained acceptance as an effective complemental, and in some cases alternative treatment to conventional oncology protocols such as surgery, radiation and chemotherapy.

However, PDT suffers from limitations related to the PS properties, light delivery and treatment monitoring which prevent its broad applicability in oncology.[9] Regarding the PSs approved in clinics, their π-delocalized tetrapyrrolic type structures enable them to be excited in the visible range. Nevertheless, such light has limited penetration depth in living tissues due to scattering and absorption by endogenous chromophores. Light excitation situated in the optical therapeutic window, between 700 and 950 nm, is considered optimal for PDT treatment since it enables to reach deeper tumors, provided that it ensures enough energy to the PS to generate singlet oxygen. Therefore, a new generation of chromophores was developed by expansion of the conjugated π-bond system of porphyrinoid compounds leading to some new PSs approved or in clinical trials.[10] A more recent approach relies on two-photon excitation of engineered PSs able to be excited in the near infrared.[11] Such excitation not only ensures higher spatial precision to the treatment but

enables also to reach deeper tumors with photons of lower energy that prevent photodamage to healthy tissue. Promising results were already reported with this new PDT modality.[12-15]

PDT treatment can also be considerably improved by combination with an imaging technique in order to optimize pre-treatment planning, to monitor drug uptake and to afford a feedback of the treatment. Theranostic drugs could bring PDT to a central position in cancer cure. Whereas various imaging techniques can be potentially used for image-guided PDT, MRI has several advantages. MRI is a noninvasive, highly versatile diagnostic tool, providing anatomical and functional images with a high temporal and spatial (down to 100 μm) resolution.[16] It is well adapted to follow the treatment since it does not use any external or inner radiation source, contrary to other imaging techniques such as X-ray, SPECT, PET and computed tomography, and it has no depth limit unlike fluorescence imaging. MR images are based on relaxation times of water protons which differ as a function of their environment (soft tissue, blood). To improve image quality, paramagnetic hydrophilic Gd(III) complexes are commonly administered as contrast agents (CAs) to decrease the relaxation rate of water protons.[17] Nevertheless, their efficiency measured by their relaxivity, r_1, (paramagnetic relaxation rate enhancement of the water protons at 1 mM concentration of CA) remains low, around 3-4 $mM^{-1}s^{-1}$ for clinical CAs such as GdDOTA (DOTA = 1,4,7,10-tetraazacyclododecane-1,4,7,10-tetraacetate). Such small hydrophilic CAs have also low tumor accumulation. To overcome these weaknesses, large doses of CA (0.1-0.3 mmol/kg) are generally administered and the development of new CAs with enhanced relaxivity and tumor specificity remains an important challenge.[18, 19]

Several mutual benefits can be expected when MRI contrast agents are conjugated to a PDT photosensitizer. The CA relaxivity should be increased due to the increased size, which reduces the tumbling rate of the molecule. The hydrophilic CA will help solubilize the aromatic,

hydrophobic PS and confer amphipathicity to the conjugate. Amphipathicity is an important property to attain high activity of the theranostic agent, as it prevents aggregation and promotes accumulation at the tumor site.

Theranostic agents combining PDT and MRI capabilities based on single molecular species have already been described. In particular, Pandey and co-workers reported several conjugates [20-22] and promising *in vivo* results with a pyropheophorbide-a PS linked to three GdDTPA complexes (DTPA: diethylenetriamine pentaacetate).[21] This conjugate enabled MR imaging in mice or rats at 10-20 times lower injection dose than Gd(III)DTPA, while being an effective PDT agent at this concentration following irradiation at 665 nm. Later, other conjugates have been also reported with variable success, depending on their chemical design, solubility and internalization.[23-31] Nanomaterials that combined PDT, MRI as well as other bioactive agents have also shown promise as theranostic agents.[32] Nevertheless, due to the controversy related to the use of nanoparticles, molecular systems seem preferable to enable better control of the effective dose of each agent for an optimized treatment.

In this context, we have previously designed and studied two theranostic molecules that associate a porphyrinic photosensitizer to Gd(III)DOTA complexes as contrast agents. They consist, respectively, of a diketopyrrolopyrrole-Zn(II) porphyrin linked to a GdDOTA complex (**DPP-ZnP-GdDOTA)**,[33] and a π-conjugated bis-Zn(II)porphyrin connected to two GdDOTA complexes, one at each side of the central porphyrin core (**GdDOTA-ZnP-ZnP-GdDOTA)** (Figure 1).[33, 34]

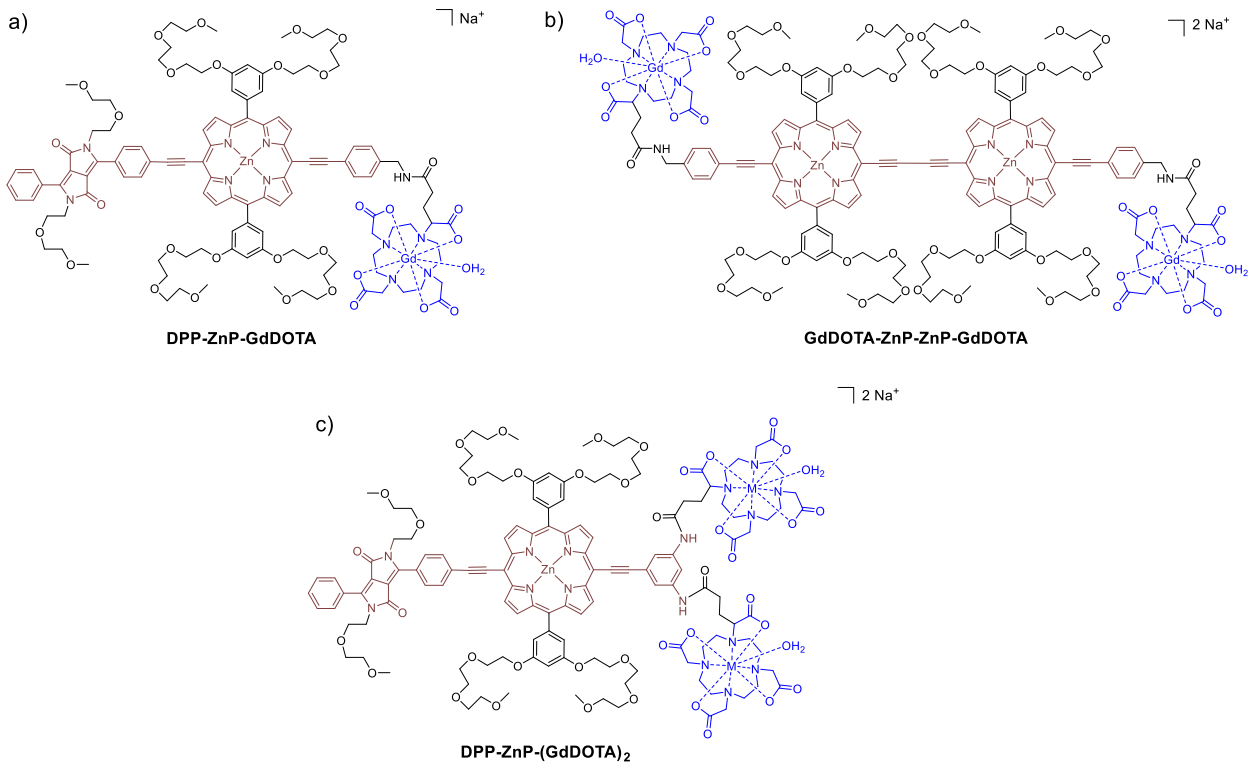

Figure 1. Theranostic agents reported previously a)[33] and b)[34], and in the present study c).

Both conjugates have shown much higher longitudinal water proton relaxivities at frequencies between 20 and 60 MHz than the clinical contrast agent GdDOTA, thanks to their decreased tumbling rate (r_1 is 18.6 $mM^{-1}s^{-1}$ and 14.4 $mM^{-1}s^{-1}$ for **DPP-ZnP-GdDOTA** and **GdDOTA-ZnP-ZnP-GdDOTA** vs. 4.34 for GdDOTA, at 25°C and 40 MHz). Interestingly, in the presence of BSA (bovine serum albumin) these relaxivities increase significantly, especially for **GdDOTA-ZnP-ZnP-GdDOTA** where r_1 doubles to reach 29.7 $mM^{-1}s^{-1}$, indicating strong supramolecular interactions with the protein, favorable for a long blood circulation time of these agents. Moreover, the large π-conjugated chromophore consisting of a porphyrin linked to a diketopyrrolopyrrole or to another porphyrin through alkyne bonds confers to these PSs strong and red-shifted absorption bands and very high two-photon absorption in the near-infrared. These particular absorption features have been exploited to induce cancer cell death following one-photon excitation in the red

(at 660 nm for **DPP-ZnP-GdDOTA**) or in the near infrared (at 740 nm for **GdDOTA-ZnP-ZnP-GdDOTA**) and two-photon excitation in the near-infrared (at 930 nm for both molecules).

These promising in-cell results have prompted us to study a novel theranostic agent, **DPP-ZnP-(GdDOTA)$_2$** that combines a diketopyrrolopyrrole-Zn(II) porphyrin PS with two GdDOTA complexes connected at the same side of the PS through *meta* positions of a phenylene unit (Figure 1c). Such a molecular design has the advantage of increasing the amphiphilicity, the reduced size can lead to a better solubility as compared to **GdDOTA-ZnP-ZnP-GdDOTA** and the two GdDOTA complexes can confer a higher relaxivity per molecule than for **DPP-ZnP-GdDOTA**. We expect that the good photophysical properties and singlet oxygen generation of the DPP-ZnP moiety will be retained and will confer good PDT activity to the bifunctional molecule. We report herein the synthesis of **DPP-ZnP-(GdDOTA)$_2$**, the photophysical characterization, and the determination of the singlet oxygen quantum yield and of the relaxometric properties. The potential of this new compound as a theranostic agent for MRI and PDT is discussed.

EXPERIMENTAL SECTION

All reagents and starting chemicals were of the best commercially available grade and used without further purification. Tetrahydrofuran was dried by distillation over sodium and benzophenone. Dry chloroform and dichloromethane were obtained by distillation over CaH_2 under argon. Analytical thin layer chromatography (TLC) was carried out on Merck aluminum backed silica gel 60 F254 plates and visualization when required was achieved using UV light. Column chromatography purifications were carried out on silica (VWR chemicals, 60-200 mesh). Size-exclusion chromatography was carried out using Bio-Beads S-X1, 200-400 mesh (Bio-Rad). NMR spectra were recorded using Bruker AVANCE 400 or 500 spectrometers. Chemical shifts are quoted as parts per million (ppm) relative to the residual peak of solvent and coupling constants

(*J*) are quoted in Hertz (Hz). To achieve full assignment of the signals the 2D-NMR techniques COSY, NOESY and ROESY have been used. In the assignments, the chemical shift (in ppm) is given first, followed, in brackets, by the multiplicity of the signal (s : singlet, d : doublet, t : triplet, m : multiplet, br s : broad signal), the number of protons implied, the value of the coupling constants in hertz if applicable, and finally the assignment. The UVIKON XL spectrophotometer was used to record UV-vis spectra. Mass spectra were obtained by using a Bruker MicroTOF spectrometer (ES-MS). ICP-AES was performed by emission spectrometry with a Vista AX CCD Simultaneous ICP-AES Varian spectrophotometer.

Compound **1** was obtained as already described by our group.[35] 1,3-diamino-5-iodobenzene was obtained by reduction of the nitro group starting from 1,3-dinitro-5-iodobenzene as described in the literature.[36] **Na_2[GdDOTAGA]**, and **Na_2[YDOTAGA]** were prepared according to a previous report.[37]

Synthesis of DPP-ZnP-$(NH_2)_2$

A solution of TBAF.$3H_2O$ (13 mg, 41.2 μmol) in anhydrous THF (1 mL) was added to a solution of compound **1** (59.5 mg, 31.8 μmol) in anhydrous THF (15 mL). The resulting solution was stirred at room temperature under argon for 25 min and then $CaCl_2$ (87 mg, 784 μmol) was added to quench the reaction. The solvents were evaporated and the crude was submitted to a silica gel column chromatography (DCM/MeOH 2 to 3%). Due to its instability, the deprotected compound obtained as a green solid was rapidly used for the next reaction. Deprotected **1** (43 mg, 25.1 μmol), $Pd(PPh_3)_4$ (6.2 mg, 5.4 μmol), CuI (2 mg, 9.9 μmol) and 1,3-diamino-5-iodobenzene (7.6 mg, 32.5 μmol) were dried under vacuum for 1h at 35°C. A solution of dry THF (5 mL) and $(i\text{Pr})_2$NH (1 mL) degassed by four freeze-pump-thaw cycles was transferred via cannula to the solids under argon. The resulting mixture was stirred at room temperature for 18 h. The solvents were

evaporated under reduced pressure and the product was purified by silica gel flash chromatography (DCM / pyridine 1% / MeOH 0 to 4 % in vol.) followed by size exclusion chromatography (Bio-Beads S-X1, DCM / pyridine 1%). Compound **DPP-ZnP-(NH_2)$_2$** was obtained as a brown-green solid in 52% yield (24 mg).

^{1}H NMR (500 MHz, $CDCl_3$/pyridine, 295 K): δ(ppm) = 3.28 (s, 12H, H1), 3.32 (s, 3H, H25) 3.38 (s, 3H, H20),3.44-3.45 (m, 2H, H24), 3.46-3.48 (m, 8H, H2), 3.50-3.51 (m, 2H, H19), 3.53-3.55 (m, 2H, H23), 3.58-3.61 (m, 10H, H18, H3), 3.66-3.68 (m, 8H, H4), 3.74-3.77 (m, 10H, H22, H5), 3.81-3.83 (m, 2H, H17), 3.91-3.93 (m, 8H, H6), 3.98-4 (m, 2H, H21), 4.04-4.06 (m, 2H, H16), 4.28-4.3 (m, 8H, H7), 6,13 (t, *J* = 2.0 Hz, 1H, p"), 6.77 (d, *J* = 2.0 Hz, 2H, o"), 6.92 (t, *J* = 2.3 Hz, 2 H, p), 7.34 (d, *J* = 2.2 Hz, 2H, o), 7.49-7.52 (m, 3H, mpx, ppx), 7.98-7.00 (m, 2H, opx), 8.11 (d, *J* = 8.3 Hz, 2H, o'), 8.23 (d, *J* = 8.3 Hz, 2H, m'), 8.88 (d, *J* = 4.7 Hz, 2H, py2 or py3), 8.92 (d, *J* = 4.4 Hz, 2H, py2 or py3), 9.63 (d, *J* = 4.3 Hz, 2H, py1 or py4), 9.65 (d , *J* = 4.2 Hz, 2H, py1 or py4).

^{13}C NMR (125 MHz, $CDCl_3$/pyridine, 295 K): δ(ppm) = 42.05, 42.41, 59.01, 59.08, 59.17, 67.78, 68.91, 69.07, 69.86, 70.48, 70.57, 70.68, 70.88, 71.86, 71.90, 91.96, 95.90, 96.73, 97.06, 99.80, 100.93, 101.87, 102,42, 109.01, 109.82, 110.06, 114.74, 122.33, 123.71, 125.53, 127.34, 128.02, 128.84, 129.37, 129.69, 130.43, 130,87, 131.24, 131.67, 132.37, 132.66, 135.74, 135.94, 144.51, 147.83, 148.39, 149,80, 149.82, 152.04, 152.13, 157.84, 162.99, 163.10.

HR ES-MS: m/z (%) 1841.6885 (100) [M+Na^+] (calcd 1841.7094 for [$C_{98}H_{112}N_8Na_1O_{22}Zn_1$]).

Synthesis of DPP-ZnP-(YDOTA)$_2$ or DPP-ZnP-(GdDOTA)$_2$

The complex **Na_2[MDOTAGA]** (73.71 μmol, 49.44 mg) was dissolved in anhydrous DMSO (3 mL) at 45 °C for 3 h. The heating was stopped and TBTU (26.20 mg, 81.60 μmol) was added

followed by DIPEA (25 μL, 147.01 µmol) and a solution of **DPP-ZnP-(NH_2)$_2$** (42 mg, 23.08 μmol) in anhydrous DMSO (3 mL). The resulting mixture was stirred at room temperature for 20 h. For **DPP-ZnP-(GdDOTA)$_2$**, a supplementary addition of TBTU (26.3 mg, 81.90 μmol) and DIPEA (24 μL, 141.13 µmol) was performed over a 24 h period. After evaporation of the solvent, the resulting solid was dissolved in CH_2Cl_2 (40 mL) and washed with H_2O (30 mL) followed by a saturated solution of NaCl (2 x 30 mL) and H_2O (30 mL). After evaporation of solvent, the solid was purified by size exclusion chromatography (Bio-Beads S-X1, CH_2Cl_2) followed by preparative TLC (DCM / MeOH / NH_3(aq): 4 / 1 / 0.25 in vol.). The product was removed from silica with the eluent and the solvent removed under reduced pressure. The resulting solid was dissolved in CH_2Cl_2 (40 mL), washed with H_2O (3 x 30 mL) and a saturated solution of NaCl (30 mL). The solid was dissolved in CH_2Cl_2 (5 mL) and precipitated with pentane (10 mL) to remove grease. Finally, the solid was dialyzed in H_2O/DMSO 1% (3 x 2 h) and the solvent removed under vacuum to afford a brown solid.

DPP-ZnP-(YDOTAGA)$_2$:

Yield: 33 %

^{1}H NMR (400 MHz, DMSO-*d6*, 298 K): δ(ppm) = 1.76-2.06 (m, 4H, H10), 2.13-3.05 (m, 50H, DOTAGA), 3.18 (s, 12H, H1), 3.19 (s, 3H, H25), 3.24 (s, 3H, H20), 3.37-3.68 (m, 44H, OCH_2), 3.84 (m, 8H, H6), 3.92 (m, 2H, H21), 4.00 (m, 2H, H16), 4.33 (m, 8H, H7), 7.022 (m, 2H, p), 7.33 (m, 4H, o), 7.61 (m, 3H, mpx, ppx), 7.86 (br, 1H, p"), 7.96 (m, 2H, opx), 8.07 (br, 2H, o"), 8.22 (d, J = 8.3 Hz, 2H, o'), 8.30 (d, J = 8.3 Hz, 2H, m'), 8.89 (d, J = 4.4 Hz, 2H, py2 or py3), 8.90 (d, J = 4.4 Hz, 2H, py2 or py3), 9.60 (d, J = 4.4 Hz, 2H, py1 or py4), 9.72 (d, J = 4.4 Hz, 2H, py1 or py4), 10.37 (br, 2H, amide).

HR ES-MS: m/z (%) 1452.4280 (100) [M^{2-}]/2 (calcd 1452.4361 for [$C_{136}H_{164}N_{16}O_{40}Y_2Zn$]).

DPP-ZnP-(GdDOTAGA)$_2$:

Yield: 56 %

UV-Vis (DMSO): λ_{max} (log ε) = 456 (5.25), 517sh, 589sh, 617sh, 668 nm (4.72).

(H_2O): λ_{max} (log ε) = 455 (5.25), 540sh, 670 nm (4.72).

HR ES-MS: m/z (%) 1521.4408 (100) $[M^{2-}]/2$ (calcd 1521.4543 for $[C_{136}H_{164}N_{16}O_{40}Gd_2Zn]$).

ICP-AES: Gd = 1.1 (± 0.1) mmol/kg, Zn = 0.58 (± 0.04) mmol/kg

Spectroscopy and photophysics

Spectroscopic grade dimethyl sulfoxide (DMSO) from Carlo Erba and dichloromethane (DCM) from Merk were used as received. Fresh tri-distilled H_2O (Millipore Milli-Q) was used to prepare the aqueous solutions. 1,3-diphenylisobenzofuran (DPBF) and Zn-phthalocyanine (ZnPc) were purchased from Aldrich.

Absorption spectra were recorded by using a PerkinElmer Lambda 650 UV-Vis spectrophotometer.

Emission spectra were collected with both an Edinburgh FLS920 fluorimeter equipped with a Peltier-cooled Hamamatsu R928 PMT (280-850 nm), and an Edinburgh FLS920 fluorimeter equipped with a Hamamatsu R5509-72 InP/InGaAs photomultiplier tube supercooled at 193 K in a liquid nitrogen cooled housing and a TM300 emission monochromator with a NIR grating blazed at 1000 nm (300–1700 nm). The spectra have been corrected for the wavelength dependent phototube response. The fluorescence quantum yields have been determined with reference to DPP-ZnP-DPP in aerated DCM as a standard (ϕ_{fl} = 0.16).[38] The concentration of the sample solutions was adjusted to have absorption values <0.10 at the excitation wavelength.

Fluorescence lifetimes were measured by means of an IBH Time Correlated Single Photon Counting apparatus, using a nanoLED excitation source at 465 nm. The analysis of the luminescence decays against time was accomplished with the DAS6 Decay Analysis Software provided by the manufacturer. The relative amplitudes of the bi-exponential fittings are reported as fractional intensities.

The singlet oxygen production quantum yield in DMSO was measured by means of a comparative method making use of DPBF as a singlet oxygen trap and ZnPc as a standard (ϕ_Δ = 0.67).[39] The solution containing a mixture of the conjugate (or the standard) and DPBF was prepared in the dark and then progressively irradiated, under continuous stirring, at 672 nm by using an irradiation setup composed by a 150 W xenon lamp (LOT) and an Omni-λ150 monochromator (Zolix) with a 16 nm slit, completed by a 635 nm cutoff filter. The light intensity was 1.0 mW cm^{-2}. The singlet oxygen quantum yield of the sample (ϕ_Δ) has been determined by using equation (1):

$$\phi_\Delta = \phi_\Delta^{Std} \frac{R.I_{abs}^{Std}}{R^{Std}.I_{abs}} \qquad (1)$$

where ϕ_Δ^{Std} is the singlet oxygen quantum yield of the standard, R and R^{Std} are the DPBF degradation rates for the sample and the standard, respectively. I_{abs} and I_{abs}^{Std} are the integrated absorption intensities, calculated as the overlap integral of the radiation source intensity and the absorption of the compound or the standard, respectively, in the spectral region defined by the slit of the monochromator, according to equation (2):[40]

$$I_{abs} = \int (1 - 10^{A_\lambda})\, I_\lambda \, d\lambda \quad (2)$$

where I_λ is the light intensity of the source and A_λ the absorbance of the compound at wavelength λ.

Estimated errors are 20% on molar absorption coefficients, 2 nm on emission and absorption peaks, 10% on lifetimes, 20% on emission quantum yields and 10% on singlet oxygen production quantum yields.

The TPA cross-section of **DPP-ZnP-(GdDOTA)$_2$** at 920 nm was obtained by the fluorescence method as described previously for parents molecules **DPP-ZnP-GdDOTA, GdDOTA-ZnP-ZnP-GdDOTA**.[33, 34, 41] Briefly, a Ti:sapphire femtosecond laser (Insight Spectra Physics) at 920 nm was used for excitation. The excitation beam was collimated over the cell length (10 mm). The fluorescence, collected at 90° of the excitation beam, was focused into an optical fiber connected to a spectrometer. The incident beam intensity was adjusted to ensure an intensity-squared dependence of the fluorescence. Calibration of the spectra was performed by comparison with Rhodamine B in MeOH.[42, 43]

Relaxometric measurements

Proton NMRD profiles (**[DPP-ZnP-(GdDOTA)$_2$]** = 0.82 mM, pH = 7.3 in 1% DMSO/H_2O) were recorded on a Stelar SMARTracer Fast Field Cycling relaxometer (0.01-10 MHz) and a Bruker WP80 NMR electromagnet adapted to variable field measurements (20-80 MHz) and controlled by a SMARTracer PC-NMR console. Higher field relaxivities were measured on Bruker AVANCE NMR spectrometers at 300 MHz, 400 MHz, and 600 MHz. The temperature was monitored by a VTC91 temperature control unit and maintained by a gas flow. The temperature

was determined by previous calibration with a Pt resistance temperature probe. The longitudinal relaxation rates ($1/T_1$) were determined in water. The least-squares fit of the ^{1}H NMRD data was performed using Visualiseur/Optimiseur (F. Yerly, *VISUALISEUR 2.3.5*, Switzerland, 1999.; F. Yerly, *OPTIMISEUR 2.3.5*, Switzerland, 1999) running on a MATLAB 8.3.0 (R2014a) platform. The relaxivity was also measured in the presence of BSA 37 g.L^{-1} for **[DPP-ZnP-(GdDOTA)$_2$]** = 0.46 mM, in H_2O (1% DMSO) at 298 K and 310 K.

Cell culture and MTT cell viability test.

HeLa cells were cultured in DMEM complete culture medium containing phenol red at 37°C with 5% CO_2. They were seeded and maintained in 25 mL Falcon culture flask or multi well LabTek (Lab-Tek® II) culture flasks. Cell viability was assessed in pentaplicate by adding a solution of 3-(4,5-dimethyl-2-thiazolyl)-2,5-diphenyl-2H-tetrazolium bromide (50 μL of a 5 mg/mL solution in DMEM by well). After an incubation period of 45 minutes, the media was removed and replaced by DMSO (150 μL). The absorbance was measured using the Safas Xenius spectrofluorimeter 96 well plates reader at 550 nm.

Dark cytotoxicity

HeLa cells were seeded in 96 wells culture plates and incubated with different concentrations of **DPP-ZnP-(GdDOTA)$_2$** (0-12 μM in DMEM with 0-0.1 % DMSO), After 24 h the cell viability was estimated using the MTT test previously described. Errors bars show standard deviation for three independent experiments.

One-photon phototoxicity tests

One-photon phototoxicity tests were performed as described in the literature using a homemade apparatus[25, 33, 34] with 800 mA high power LED Deep Red (640-660 nm) (FutureEden™) adapted for Corning® 96 well special optic plates. Cells were cultured 1 day in these 96 well plates and incubated with a solution of **DPP-ZnP-(GdDOTA)$_2$** (2 μM in DMEM with 0.01 % DMSO) for 24 h. The medium was replaced by new DMEM free of sensitizer and the plates were irradiated for 15 or 30 min. The LEDs power was measured with a Thorlabs PM100D power-meter. The cell viability was estimated 24 h after irradiation using the MTT test previously described. Errors bars show standard deviation for three independent experiments.

RESULTS AND DISCUSSION

Design and synthesis

Two conjugates **DPP-ZnP-(MDOTA)$_2$** with M = Gd (III) or Y(III) were synthesized (Figure 2). The diamagnetic **DPP-ZnP-(YDOTA)$_2$** was prepared to optimize the reaction conditions used to synthesize the targeted paramagnetic **DPP-ZnP-(GdDOTA)$_2$**. A modular approach was chosen to connect in the last step of the synthesis the PS moiety **DPP-ZnP-(NH$_2$)$_2$** to two Gd(III) or Y(III) complexes **Na$_2$[MDOTAGA]** (DOTAGA : 1,4,7,10-tetraazacyclododecane-1-glutaric-4,7,10-triacetate) by the formation of amide bonds.

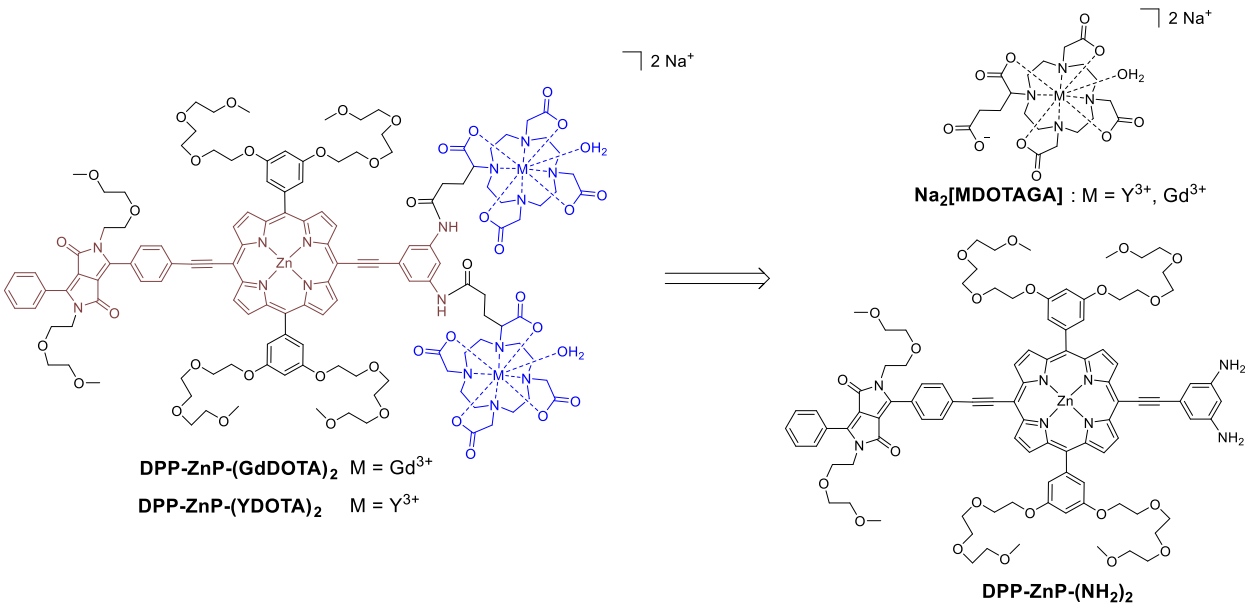

Figure 2. Retrosynthetic approach used to conjugate the MRI contrast agents to the PS.

The porphyrin precursor **DPP-ZnP-(NH$_2$)$_2$** was readily obtained starting from the diketopyrrolopyrrole-porphyrin-conjugate **1** previously reported (Scheme 1).[35] Compound **1** was submitted to a Sonogashira cross-coupling reaction with 5-iodobenzene-1,3-diamine under standard conditions to afford **DPP-ZnP-(NH$_2$)$_2$** in 52 % yield after purification by column chromatography. The second precursor, Na$_2$[MDOTAGA] was obtained quantitatively by complexation of DOTAGA with YCl_3 or $GdCl_3$ as already reported.[37]

The final coupling reaction between **DPP-ZnP-(NH$_2$)$_2$** and 3 equiv. of **Na$_2$[MDOTAGA]** was performed in mild conditions to prevent possible demetallation reactions. In the case of the reaction involving **Na$_2$[GdDOTAGA]**, reactants were mixed at room temperature for 40 h in dry DMSO in the presence of an activating agent *O*-(benzotriazol-1-yl)-N,N,N',N'-tetramethyluronium tetrafluoroborate (TBTU) and *N*,*N*-diisopropylethylamine (DIPEA) as a base. Purification was achieved by size-exclusion chromatography followed by preparative thin layer chromatography

and dialysis. The desired theranostic compound **DPP-ZnP-(GdDOTA)$_2$** was isolated as a sodium salt in 56% yield. It was characterized by high-resolution ESI-mass spectrometry with the isotopic profile of the ionic species $[M\text{-}2H_2O]^{2-}/2$, detected as the major species in accordance with the calculated profile (see Fig. S6). ICP-AES experiment gave a 1:2 ratio for Zn/Gd confirming the metalation of the porphyrin and DOTA ligands (see Table S1).

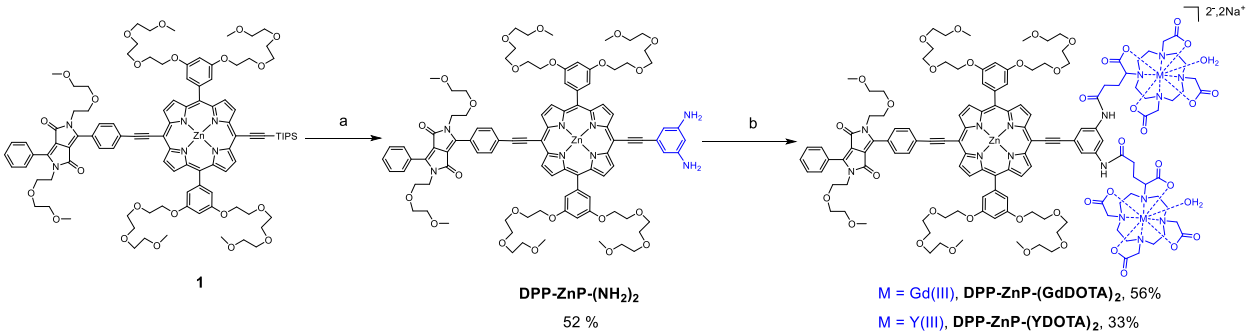

Scheme 1. Reagents and conditions: a) 5-iodobenzene-1,3-diamine, $Pd(PPh_3)_4$, CuI, $(iPr)_2NH$; b) **Na_2[GdDOTAGA]** or **Na_2[YDOTAGA],** TBTU, DIPEA, DMSO.

Relaxivity measurements

The efficacy (relaxivity) of a contrast agent is dependent upon several microscopic parameters, which are linked to the structure of the molecule. The most important microscopic parameters are (1) the number of water molecules directly coordinated to the Gd^{3+} (hydration number, q), (2) the exchange rate of those water molecules with the bulk (k_{ex}), (3) the rotational correlation time of the complex (τ_R), and (4) the parameters describing electronic relaxation (τ_V and Δ^2). The relation between those parameters is described by the Solomon-Bloembergen and Morgan (SBM) theory of paramagnetic relaxation. In the case of contrast agents with high molecular weight such as **DPP-ZnP-(GdDOTA)$_2$**, it is often necessary to use the Lipari-Szabo approach to describe the rotational

dynamics. This allows for separating a fast local motion (τ_l, around the Gd^{3+} complex) and a slow global motion (τ_g) for the whole conjugate. The degree of spatial restriction of the local with respect to the global motion is given by a generalized, model independent order parameter, S^2. The paramagnetic relaxation mechanism is dependent upon the magnetic field, therefore contrast agents are often characterized by their NMRD (Nuclear Magnetic Relaxation Dispersion) profiles representing the relaxivity as a function of the magnetic field.

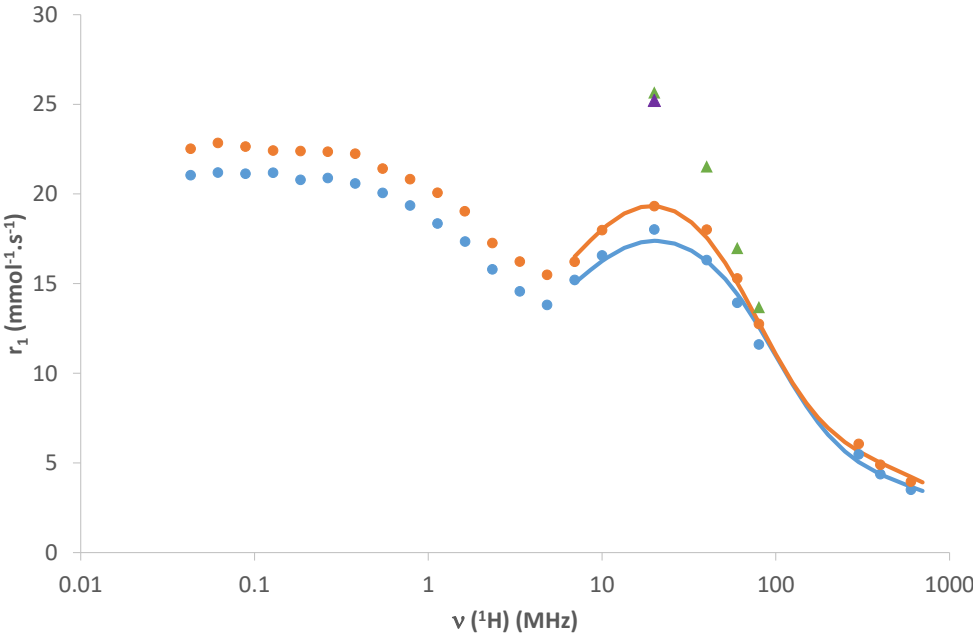

Figure 3. ^1H Nuclear Magnetic Relaxation Dispersion (NMRD) profiles for **[DPP-ZnP-(GdDOTA)$_2$]** (0.82 mM, pH = 7.3) at 25°C (●) and 37°C (●) in H_2O (1% DMSO). The continuous lines represent the fitted curves. Relaxivities obtained in the presence of BSA 37 $g.L^{-1}$ for **[DPP-ZnP-(GdDOTA)$_2$]** at 0.46 mM, in H_2O (1% DMSO) at 298 K (▲) and 310 K (▲).

NMRD profiles have been recorded for **DPP-ZnP-(GdDOTA)$_2$** in water with 1% of DMSO (to ensure the full solubilisation of the complex), at pH = 7.3 and at 298 and 310 K (Figure 3). The

relaxivity at 20 MHz and 298 K is 19.32, which is in the same range of magnitude as those for **GdDOTA-ZnP-ZnP-GdDOTA** and **DPP-ZnP-GdDOTA** (Table 1). The NMRD profiles show the typical hump at intermediate magnetic fields, which is characteristic of slowly rotating species, in accordance with the size of the conjugate.

The NMRD data have been fitted with the SBM theory including the Lipari-Szabo approach (see ESI for the equations). The fitting was restricted to frequencies above 6 MHz, as at lower magnetic fields, the SBM theory fails in describing electronic parameters and rotational dynamics of slowly rotating objects. The main parameters obtained from those fittings are shown in Table 1 together with those of the other porphyrinic systems for comparison. The full parameter set is given in Table S2. In the fitting procedure, the hydration number was 1, and the water exchange parameters have been fixed to the values reported for **GdDOTA**.[44] The local rotational correlation time, $\tau_l^{298} = 165\ ps$, and the order parameter ($S^2 = 0.30$) are in the same order of magnitude as those for the other porphyrinic systems. They are both quite low and imply a significant flexibility of the Gd(III) chelates within this molecule, likely resulting from the flexibility of the two methylene groups in the linker between the chelates and the phenyl group.

The global rotational correlation time, $\tau_g^{298} = 2250\ ps$ is slightly lower than that of **DPP-ZnP-GdDOTA** ($\tau_g^{298} = 2640\ ps$), and significantly higher than the value reported for **GdDOTA-ZnP-ZnP-GdDOTA** ($\tau_g^{298} = 1360\ ps$), in accordance with the trend of the relaxivities found at 25°C and 20 MHz for the three systems (Table 1). **DPP-ZnP-GdDOTA** has the lowest molecular weight and still the highest relaxivity, which was ascribed to some aggregation in aqueous solution. In contrast, **GdDOTA-ZnP-ZnP-GdDOTA** has the highest molecular weight and the lowest relaxivity, and we had previously shown that aggregation remained limited for this system. For **DPP-ZnP-(GdDOTA)$_2$**, the elevated relaxivity values in the range of 20-60 MHz, close to those

of **DPP-ZnP-GdDOTA,** likely point to the presence of aggregates in solution. Although aggregation was not further investigated by relaxivity measurements, it was also suggested by the photophysical data (*vida supra*).

We also measured the relaxivity in the presence of bovine serum albumin (37 $g.L^{-1}$) at 298 K 20 MHz, and at 310 K in the range of 20-80 MHz. A relaxivity increase of 30 and 40 % is obtained upon addition of BSA at 298 and 310 K, respectively, indicative of an interaction between **DPP-ZnP-(GdDOTA)$_2$** and the protein. The similar relaxivities observed at 298 and 310 K in the presence of BSA (at 20 MHz) suggest that we attain the regime where relaxivity starts to be limited by slow water exchange as well and not only by fast rotation.

Table 1. Best fit parameters obtained from the fitting of the ^{1}H NMRD profile to the SBM theory, including the Lipari-Szabo approach for internal flexibility.

Parameters	**DPP-ZnP-(GdDOTA)$_2$** in H_2O + 1% DMSO	**GdDOTA-ZnP-ZnP-GdDOTA** in H_2O + 2% pyridine[b]	**DPP-ZnP-GdDOTA** in H_2O[c]
M_w	3082 Da	3913 Da	2471 Da
r_1 *(mM^{-1}s^{-1}; 20 MHz, 25°C)*	19.32	14.33	19.94
q^a	1	1	1
k_{ex}^{298} (10^6 s^{-1})[a]	4.1	4.1	4.1
$\Delta H^{\neq}$ ($kJ.mol^{-1}$)[a]	49.8	49.8	49.8
E_l ($kJ.mol^{-1}$)	21 ± 6	26	40
τ_l^{298} (ps)	165 ± 13	207	245
E_g ($kJ.mol^{-1}$)	19 ± 5	25	14
τ_g^{298} (ps)	2250 ± 250	1360	2640
S^2	0.30 ± 0.03	0.30	0.26

[a]Fixed in the fit. [b]From ref 34. [c]From ref 33.

Photophysical and characterization and singlet oxygen production

A complete photophysical characterization of the conjugate has been performed in DMSO and H_2O in order to assess important characteristics for its applications as a theranostic agent in biological environments, such as absorption and emission features, fluorescence quantum yield and singlet oxygen production.

The absorption spectrum of **DPP-ZnP-(GdDOTA)$_2$**, measured in both solvents, is reported in Figure 4a and the relevant parameters are summarized in Table 2. The absorption features in DMSO resemble those of the parent compound **DPP-ZnP-GdDOTA**,[33] with an intense Soret band at 455 nm and a single Q-band at 670 nm with high absorption (ε of the order of 60 000 M^{-1} cm^{-1}). The latter property is of great relevance for the use of the conjugate as one-photon PS upon excitation at 660 nm (see below). The spectrum in H_2O is only slightly broader (Figure 4a), indicating moderate aggregation phenomena in this solvent.

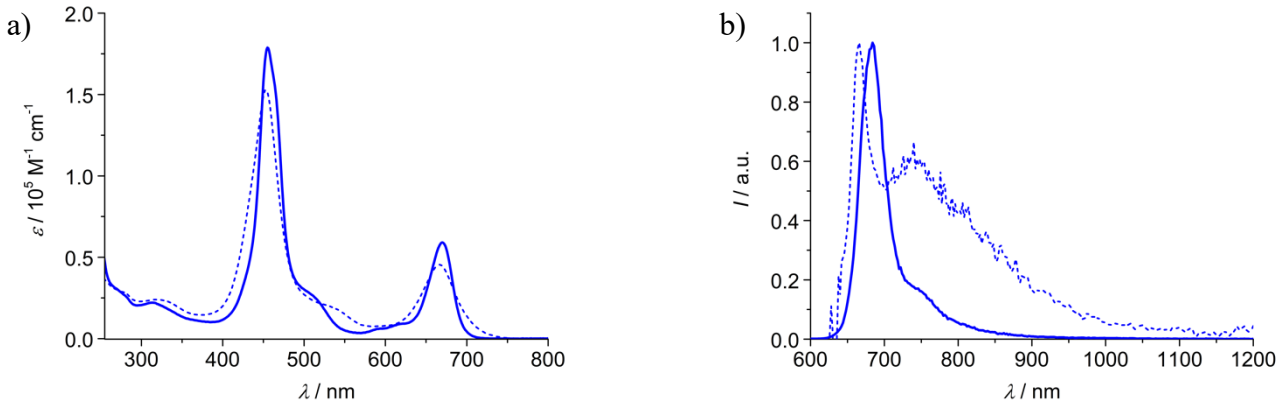

Figure 4. Absorption a) and normalized corrected emission b) spectra of **DPP-ZnP-(GdDOTA)$_2$** in DMSO (full line) and H_2O (dotted line). Excitation at 590 nm.

Table 2. Absorption and luminescence data for **DPP-ZnP-(GdDOTA)$_2$** at room temperature

	λ^{max}_{abs} / nm	ε / M^{-1} cm^{-1}	λ^{max}_{fl} / nm[a]	ϕ_{fl} [b]	τ / ns [c]	ϕ_{Δ} [d]
DMSO	455	179 000	684, 746 sh	0.13	0.90	0.58
	670	59 000				
H_2O	453	153 000	666, 742	4.7×10^{-3}	< 0.2 (60%); 1.01 (40%)	-
	667	45 400				

[a] From corrected emission spectra. [b] Fluorescence quantum yields, measured with reference to DPP-ZnP-DPP in aerated DCM (ϕ_{fl} = 0.16).[38] [c] Fluorescence lifetimes, excitation at 465 nm. [d] Singlet oxygen production quantum yields (see the Experimental Section for details).

DPP-ZnP-(GdDOTA)$_2$ shows, in DMSO, a fluorescence spectrum peaking at 684 nm, with quantum yield of 0.13 and excited state lifetime of 0.90 ns (Figure 4b and Table 2). The emission spectral range close to the NIR region is ascribed to the extended conjugation of the porphyrin core, due to the presence of the ethynyl linkers and the lateral DPP and phenyl units, that lowers the energy of the emissive singlet state, as observed for the parent **DPP-ZnP-GdDOTA**.[33] The luminescence parameters of **DPP-ZnP-(GdDOTA)$_2$** are very close to those of the parent compound, indicating that the addition of a second GdDOTA complex is not affecting the fluorescence features of the porphyrin system. In H_2O a peak ascribed to the porphyrin fluorescence is observed at 666 nm, accompanied by a broad shoulder extending in the NIR (Figure 4b). The *ca.* 30 times lower quantum yield and the bi-exponential fluorescence decay observed in H_2O (Table 1) confirm the presence of aggregates. The emission spectrum, however, is not completely featureless as observed for **DPP-ZnP-GdDOTA**,[33] suggesting a better solubility of the present conjugate in H_2O. Indeed, the excitation spectrum of **DPP-ZnP-(GdDOTA)$_2$** collected at 740 nm reasonably superimpose the absorption spectrum in both solvents (Figure S7).

The singlet oxygen production quantum yield has been measured in DMSO by using 1,3-diphenylisobenzofuran (DPBF) as a singlet oxygen trap and with reference to Zn-phthalocyanine (ZnPc) as a standard (ϕ_Δ = 0.67)[39] (see Experimental Section for details). The evolution of the absorption spectrum of a mixture of **DPP-ZnP-(GdDOTA)$_2$** and DPBF has been followed upon irradiation at 672 nm (Figure S8). The conjugate is not degrading upon irradiation, and its constant absorption contribution can be subtracted by the spectra of the mixture to follow the decrease of the DPBF band peaking at 417 nm (Figure S8). The rate of DPBF conversion is derived as the slope of the linear fitting of the trend of its absorbance at 417 nm as a function of time (Figure S8). By comparison with the reaction rate measured in the same way for the standard ZnPc (Figure S9), and taking into consideration the integrated absorption at the excitation wavelength of both the sample and the standard, a value of ϕ_Δ = 0.58 is derived for **DPP-ZnP-(GdDOTA)$_2$**. This value is slightly lower than that measured for **DPP-ZnP-GdDOTA** (ϕ_Δ = 0.68)[33] but in line with that of the parent **DPP-ZnP** conjugate (ϕ_Δ = 0.54),[38] and indicative of a good potential activity of **DPP-ZnP-(GdDOTA)$_2$** as a phototoxic agent.

In addition, to evaluate the potential of the conjugate as a two-photon sensitizer for PDT, the two-photon absorption cross section of **DPP-ZnP-(GdDOTA)$_2$** was determined in **DMSO** solution. At 920 nm, the measured value of σ_2 was 650 GM, a value slightly lower than the one of the previously described **DPP-ZnP-GdDOTA** endowed with only one Gd(III)DOTA complex (σ_2 = 950 GM).[33]

Biological tests on cell culture

To investigate the cell localization of **DPP-ZnP-(GdDOTA)$_2$** confocal microscopy experiments were performed on HeLa cells. The nucleus, mitochondria and lysosomes were counter stained with commercial organelle targeting dyes (Hoechst 33342, MitoTracker™ Green and LysoTracker™ Green, respectively). A clear localization of the theranostic compound was observed in the lysosomes whereas no fluorescence was detected in the mitochondria and nucleus (Figure 5).

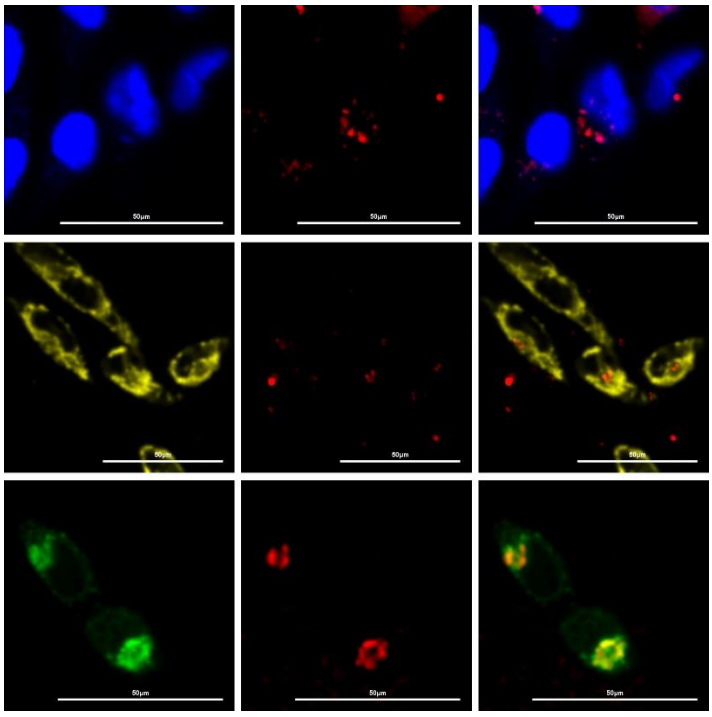

Figure 5. Confocal images of HeLa cells stained with **DPP-ZnP-(GdDOTA)$_2$ (1 μM)** and Hoechst 33342 (top line) MitoTracker (middle line) and LysoTracker (bottom line). Left column: organelle specific dyes, middle column: **DPP-ZnP-(GdDOTA)$_2$**, right column: merged images (Scale bar is 50 μm).

Dark toxicity was also investigated on HeLa cells after 24 h of incubation with **DPP-ZnP-(GdDOTA)$_2$**, using the MTT (3-(4,5-dimethylthiazol-2-yl)-2,5-diphenyl tetrazolium bromide)) cell test (Figure 6). The theranostic agent exhibited a dark toxicity of 50 % at 12 μM concentration and a low toxicity (< 10-20 %) at 2 μM, the concentration chosen for the phototoxicity experiments.

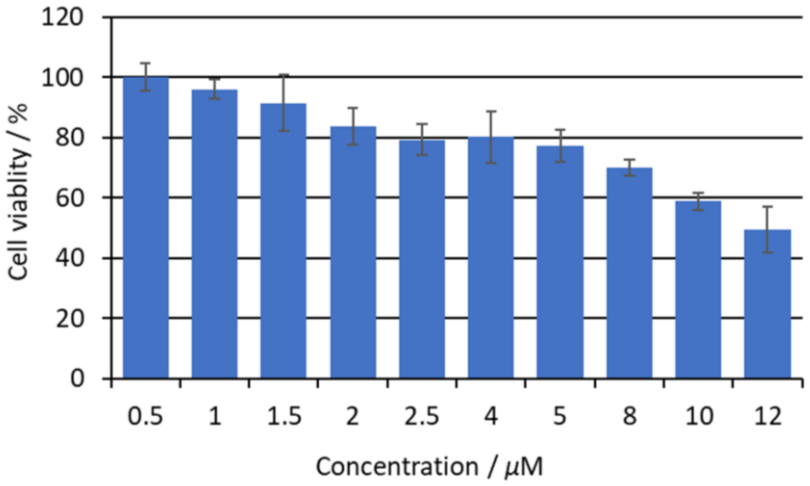

Figure 6. Phototoxicity of **DPP-ZnP-(GdDOTA)$_2$** on HeLa cell cultures after 24 h incubation.

Phototoxicity induced by light irradiation was assessed using a LED setup as previously described.[12, 33] HeLa cells were incubated with the **DPP-ZnP-(GdDOTA)$_2$** for 24 h followed by irradiation at 660 nm with an irradiance of 36 mW/cm². The toxicity was then evaluated using an MTT assay (Figure 7). After 15 min irradiation the phototoxicity was evaluated at 30 % and by increasing the irradiation time to 30 min, a much stronger phototoxicity was obtained, reaching 70 %. The light dose to induce 50 % cell death (LD_{50}), around 45 Jcm^{-2} (at 2 μM), is higher than the one, 9 Jcm^{-2}, reported for **DPP-ZnP-GdDOTA**.[33] This can be due to a cell penetration decrease of the dianionic **DPP-ZnP-(GdDOTA)$_2$**, as compared to the monoanionic complex **DPP-ZnP-GdDOTA.**[33] Noteworthy, the LD_{50} following excitation at 660 nm is close to the one of the

dianionic **GdDOTA-ZnP-ZnP-GdDOTA,** 40 Jcm^{-2} which epsilon is two times higher (1.17 x 10^5 M^{-1} cm^{-1}) at the excitation wavelength of 740 nm but which singlet oxygen generation, Φ_Δ= 0.36, is lower in DMSO. Both these dianionic theranostic agents are thus able to induce phototoxicity while other compounds lose this capacity when several Gd(III) complexes are linked to the PS due to their higher hydrophilicity and the increased charges repulsion with the anionic cell membrane which prevents efficient internalization.[24]

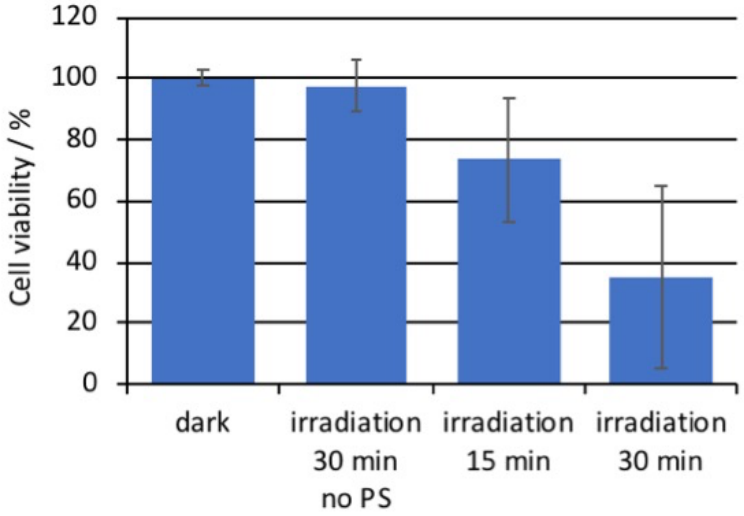

Figure 7. Phototoxicity of **DPP-ZnP-(GdDOTA)$_2$** (2 μM) on HeLa cell cultures after irradiation at 660 nm (with the theranostic agent and no irradiation (dark); 30 min irradiation without the theranostic agent; with the theranostic agent and irradiation for 15 mn; with the theranostic agent and irradiation 30 min).

CONCLUSION

Two GdDOTA contrast agents for MRI were successfully linked to a π-conjugated diketopyrrolopyrrole-Zn(II)porphyrin photosensitizer. The water soluble conjugate **DPP-ZnP-(GdDOTA)$_2$** features a high relaxivity of 19.32 $mM^{-1}s^{-1}$ (20 MHz, 298 K) per Gd ion, close to the

one of **DPP-ZnP-GdDOTA**. This relaxivity value, five times higher than those of clinical contrast agents, is attributed to the medium size of the molecule and to its self-aggregation at a millimolar concentration. Nevertheless, the two Gd complexes provide this contrast agent with a molecular relaxivity twice as high as for **DPP-ZnP-GdDOTA** which is beneficial for imaging at lower concentration. On the other hand, the 30% increase in relaxivity obtained for **DPP-ZnP-(GdDOTA)$_2$** in presence of serum albumin should lead to a longer blood circulation favorable to its tumor accumulation. The conjugate has also shown good singlet oxygen generation ability (Φ_Δ= 0.58) for PDT and also remarkable fluorescence emission (Φ_{fl}= 0.13). Its amphipathic nature favored its internalization in HeLa cells and its accumulation in lysosomes could be detected by its fluorescence. Phototoxicity was found to be high, with 70% of cell death after 30 mn irradiation in the red. Combined with a good two-photon absorption cross section (650 GM) at 920 nm, this new PDT-MRI theranostic agent is also promising for two-photon excited PDT in the near-infrared.

Acknowledgements

The icFRC (http://www.icfrc.fr) and LabEx CSC are gratefully acknowledged for financial support. The Ministry of Education and Research is acknowledged for a Ph.D. fellowship to S.J.. The Italian CNR (Project ”PHEEL”) is also acknowledged.

ASSOCIATED CONTENT

Supporting Information.

NMR spectra and HR-MS data, photophysical measurements, singlet oxygen quantum yield determination and relaxometric measurements.

REFERENCES

1. Kelkar, S. S.; Reineke, T. M. Theranostics: Combining Imaging and Therapy. *Bioconjugate Chem.* **2011,** 22 (10), 1879-1903 DOI: 10.1021/bc200151q.
2. Kumar, R.; Shin, W. S.; Sunwoo, K.; Kim, W. Y.; Koo, S.; Bhuniya, S.; Kim, J. S. Small conjugate-based theranostic agents: an encouraging approach for cancer therapy. *Chem. Soc. Rev.* **2015,** 44 (19), 6670-6683 DOI: 10.1039/C5CS00224A.
3. Terreno, E.; Uggeri, F.; Aime, S. Image guided therapy: The advent of theranostic agents. *J. Controlled Release* **2012,** 161 (2), 328-337 DOI: https://doi.org/10.1016/j.jconrel.2012.05.028.
4. Rai, P.; Mallidi, S.; Zheng, X.; Rahmanzadeh, R.; Mir, Y.; Elrington, S.; Khurshid, A.; Hasan, T. Development and applications of photo-triggered theranostic agents. *Adv. Drug Delivery Rev.* **2010,** 62 (11), 1094-1124 DOI: https://doi.org/10.1016/j.addr.2010.09.002.
5. van Straten, D.; Mashayekhi, V.; de Bruijn, H.; Oliveira, S.; Robinson, D. Oncologic Photodynamic Therapy: Basic Principles, Current Clinical Status and Future Directions. *Cancers* **2017,** 9 (12), 19 DOI: 10.3390/cancers9020019.
6. O'Connor, A. E.; Gallagher, W. M.; Byrne, A. T. Porphyrin and Nonporphyrin Photosensitizers in Oncology: Preclinical and Clinical Advances in Photodynamic Therapy. *Photochem. Photobiol.* **2009,** 85 (5), 1053-1074 DOI: 10.1111/j.1751-1097.2009.00585.x.
7. Agostinis, P.; Berg, K.; Cengel, K. A.; Foster, T. H.; Girotti, A. W.; Gollnick, S. O.; Hahn, S. M.; Hamblin, M. R.; Juzeniene, A.; Kessel, D.; Korbelik, M.; Moan, J.; Mroz, P.; Nowis, D.; Piette, J.; Wilson, B. C.; Golab, J. Photodynamic therapy of cancer: An update. *Ca-Cancer J. Clin.* **2011,** 61 (4), 250-281 DOI: 10.3322/caac.20114.
8. Fan, W.; Huang, P.; Chen, X. Overcoming the Achilles' heel of photodynamic therapy. *Chem. Soc. Rev.* **2016,** 45 (23), 6488-6519 DOI: 10.1039/C6CS00616G.
9. Abrahamse, H.; Hamblin, Michael R. New photosensitizers for photodynamic therapy. *Biochem. J.* **2016,** 473 (4), 347-364 DOI: 10.1042/bj20150942.
10. Baskaran, R.; Lee, J.; Yang, S.-G. Clinical development of photodynamic agents and therapeutic applications. *Biomater. Res.* **2018,** 22 (1), 25 DOI: 10.1186/s40824-018-0140-z.
11. Bolze, F.; Jenni, S.; Sour, A.; Heitz, V. Molecular photosensitisers for two-photon photodynamic therapy. *Chem. Commun.* **2017,** 53 (96), 12857-12877 DOI: 10.1039/C7CC06133A.
12. Jenni, S.; Sour, A.; Bolze, F.; Ventura, B.; Heitz, V. Tumour-targeting photosensitisers for one- and two-photon activated photodynamic therapy. *Org. Biomol. Chem.* **2019,** 17, 6585-6594 DOI: 10.1039/C9OB00731H.
13. Starkey, J. R.; Rebane, A. K.; Drobizhev, M. A.; Meng, F.; Gong, A.; Elliott, A.; McInnerney, K.; Spangler, C. W. New Two-Photon Activated Photodynamic Therapy Sensitizers Induce Xenograft Tumor Regressions after Near-IR Laser Treatment through the Body of the Host Mouse. *Clin. Cancer Res.* **2008,** 14 (20), 6564-6573 DOI: 10.1158/1078-0432.ccr-07-4162.
14. Collins, H. A.; Khurana, M.; Moriyama, E. H.; Mariampillai, A.; Dahlstedt, E.; Balaz, M.; Kuimova, M. K.; Drobizhev, M.; Yang, V. X. D.; Phillips, D.; Rebane, A.; Wilson, B. C.;

Anderson, H. L. Blood-vessel closure using photosensitizers engineered for two-photon excitation. *Nat. Photonics* **2008,** 2, 420 DOI: 10.1038/nphoton.2008.100
15. Sun, Z.; Zhang, L.-P.; Wu, F.; Zhao, Y. Photosensitizers for Two-Photon Excited Photodynamic Therapy. *Adv. Funct. Mater.* **2017,** 27 (48), 1704079 DOI: 10.1002/adfm.201704079.
16. Upputuri, P. K.; Sivasubramanian, K.; Mark, C. S. K.; Pramanik, M. Recent Developments in Vascular Imaging Techniques in Tissue Engineering and Regenerative Medicine. *BioMed Res. Int.* **2015,** 9 DOI: 10.1155/2015/783983.
17. Hermann, P.; Kotek, J.; Kubíček, V.; Lukeš, I. Gadolinium(iii) complexes as MRI contrast agents: ligand design and properties of the complexes. *Dalton Trans.* **2008,** (23), 3027-3047 DOI: 10.1039/B719704G.
18. De León-Rodríguez, L. M.; Martins, A. F.; Pinho, M. C.; Rofsky, N. M.; Sherry, A. D. Basic MR relaxation mechanisms and contrast agent design. *Journal of Magnetic Resonance Imaging* **2015,** 42 (3), 545-565 DOI: 10.1002/jmri.24787.
19. Lacerda, S.; Tóth, É. Lanthanide Complexes in Molecular Magnetic Resonance Imaging and Theranostics. *ChemMedChem* **2017,** 12 (12), 883-894 DOI: 10.1002/cmdc.201700210.
20. Li, G.; Slansky, A.; Dobhal, M. P.; Goswami, L. N.; Graham, A.; Chen, Y.; Kanter, P.; Alberico, R. A.; Spernyak, J.; Morgan, J.; Mazurchuk, R.; Oseroff, A.; Grossman, Z.; Pandey, R. K. Chlorophyll-a Analogues Conjugated with Aminobenzyl-DTPA as Potential Bifunctional Agents for Magnetic Resonance Imaging and Photodynamic Therapy. *Bioconjugate Chem.* **2005,** 16 (1), 32-42 DOI: 10.1021/bc049807x.
21. Spernyak, J. A.; White, W. H.; Ethirajan, M.; Patel, N. J.; Goswami, L.; Chen, Y.; Turowski, S.; Missert, J. R.; Batt, C.; Mazurchuk, R.; Pandey, R. K. Hexylether Derivative of Pyropheophorbide-a (HPPH) on Conjugating with 3Gadolinium(III) Aminobenzyldiethylenetriaminepentaacetic Acid Shows Potential for in Vivo Tumor Imaging (MR, Fluorescence) and Photodynamic Therapy. *Bioconjugate Chem.* **2010,** 21 (5), 828-835 DOI: 10.1021/bc9005317.
22. Goswami, L. N.; White, W. H.; Spernyak, J. A.; Ethirajan, M.; Chen, Y.; Missert, J. R.; Morgan, J.; Mazurchuk, R.; Pandey, R. K. Synthesis of Tumor-Avid Photosensitizer−Gd(III)DTPA Conjugates: Impact of the Number of Gadolinium Units in T1/T2 Relaxivity, Intracellular localization, and Photosensitizing Efficacy. *Bioconjugate Chem.* **2010,** 21 (5), 816-827 DOI: 10.1021/bc9005305.
23. Hindré, F.; Plouzennec, M. L.; de Certaines, J. D.; Foultier, M. T.; Patrice, T.; Simonneaux, G. Tetra-p-aminophenylporphyrin conjugated with Gd-DTPA: Tumor-specific contrast agent for MR imaging. *Journal of Magnetic Resonance Imaging* **1993,** 3 (1), 59-65 DOI: 10.1002/jmri.1880030111.
24. Song, Y.; Zong, H.; Trivedi, E. R.; Vesper, B. J.; Waters, E. A.; Barrett, A. G. M.; Radosevich, J. A.; Hoffman, B. M.; Meade, T. J. Synthesis and Characterization of New Porphyrazine-Gd(III) Conjugates as Multimodal MR Contrast Agents. *Bioconjugate Chem.* **2010,** 21 (12), 2267-2275 DOI: 10.1021/bc1002828.
25. Sour, A.; Jenni, S.; Ortí-Suárez, A.; Schmitt, J.; Heitz, V.; Bolze, F.; Loureiro de Sousa, P.; Po, C.; Bonnet, C. S.; Pallier, A.; Tóth, É.; Ventura, B. Four Gadolinium(III) Complexes Appended to a Porphyrin: A Water-Soluble Molecular Theranostic Agent with Remarkable Relaxivity Suited for MRI Tracking of the Photosensitizer. *Inorg. Chem.* **2016,** 55 (9), 4545-4554 DOI: 10.1021/acs.inorgchem.6b00381.

26. Aydın Tekdaş, D.; Garifullin, R.; Şentürk, B.; Zorlu, Y.; Gundogdu, U.; Atalar, E.; Tekinay, A. B.; Chernonosov, A. A.; Yerli, Y.; Dumoulin, F.; Guler, M. O.; Ahsen, V.; Gürek, A. G. Design of a Gd-DOTA-Phthalocyanine Conjugate Combining MRI Contrast Imaging and Photosensitization Properties as a Potential Molecular Theranostic. *Photochem. Photobiol.* **2014,** 90 (6), 1376-1386 DOI: 10.1111/php.12332.
27. Luo, J.; Chen, L.-F.; Hu, P.; Chen, Z.-N. Tetranuclear Gadolinium(III) Porphyrin Complex as a Theranostic Agent for Multimodal Imaging and Photodynamic Therapy. *Inorg. Chem.* **2014,** 53 (8), 4184-4191 DOI: 10.1021/ic500238s.
28. Haroon Ur, R.; Umar, M. N.; Khan, K.; Anjum, M. N.; Yaseen, M. Synthesis and relaxivity measurement of porphyrin-based Magnetic Resonance Imaging (MRI) contrast agents. *J. Struct. Chem.* **2014,** 55 (5), 910-915 DOI: 10.1134/S0022476614050163.
29. Ke, X.-S.; Tang, J.; Yang, Z.-S.; Zhang, J.-L. β-conjugation of gadolinium(III) DOTA complexes to zinc(II) porpholactol as potential multimodal imaging contrast agents. *J. Porphyrins Phthalocyanines* **2014,** 18 (10n11), 950-959 DOI: 10.1142/S1088424614500758.
30. Wu, B.; Li, X.-Q.; Huang, T.; Lu, S.-T.; Wan, B.; Liao, R.-F.; Li, Y.-S.; Baidya, A.; Long, Q.-Y.; Xu, H.-B. MRI-guided tumor chemo-photodynamic therapy with Gd/Pt bifunctionalized porphyrin. *Biomater. Sci.* **2017,** 5 (9), 1746-1750 DOI: 10.1039/C7BM00431A.
31. Yuzhakova, D. V.; Lermontova, S. A.; Grigoryev, I. S.; Muravieva, M. S.; Gavrina, A. I.; Shirmanova, M. V.; Balalaeva, I. V.; Klapshina, L. G.; Zagaynova, E. V. In vivo multimodal tumor imaging and photodynamic therapy with novel theranostic agents based on the porphyrazine framework-chelated gadolinium (III) cation. *Biochim. Biophys. Acta, Gen. Subj.* **2017,** 1861 (12), 3120-3130 DOI: https://doi.org/10.1016/j.bbagen.2017.09.004.
32. Jokerst, J. V.; Gambhir, S. S. Molecular Imaging with Theranostic Nanoparticles. *Acc. Chem. Res.* **2011,** 44 (10), 1050-1060 DOI: 10.1021/ar200106e.
33. Schmitt, J.; Heitz, V.; Sour, A.; Bolze, F.; Kessler, P.; Flamigni, L.; Ventura, B.; Bonnet, C. S.; Tóth, É. A Theranostic Agent Combining a Two-Photon-Absorbing Photosensitizer for Photodynamic Therapy and a Gadolinium(III) Complex for MRI Detection. *Chem. - Eur. J.* **2016,** 22 (8), 2775-2786 DOI: 10.1002/chem.201503433.
34. Schmitt, J.; Jenni, S.; Sour, A.; Heitz, V.; Bolze, F.; Pallier, A.; Bonnet, C. S.; Tóth, É.; Ventura, B. A Porphyrin Dimer–GdDOTA Conjugate as a Theranostic Agent for One- and Two-Photon Photodynamic Therapy and MRI. *Bioconjugate Chem.* **2018,** 29 (11), 3726-3738 DOI: 10.1021/acs.bioconjchem.8b00634.
35. Schmitt, J.; Heitz, V.; Sour, A.; Bolze, F.; Ftouni, H.; Nicoud, J.-F.; Flamigni, L.; Ventura, B. Diketopyrrolopyrrole-Porphyrin Conjugates with High Two-Photon Absorption and Singlet Oxygen Generation for Two-Photon Photodynamic Therapy. *Angew. Chem., Int. Ed.* **2015,** 54 (1), 169-173 DOI: 10.1002/anie.201407537.
36. Lux, J.; Chan, M.; Vander Elst, L.; Schopf, E.; Mahmoud, E.; Laurent, S.; Almutairi, A. Metal chelating crosslinkers form nanogels with high chelation stability. *J. Mater. Chem. B* **2013,** 1 (46), 6359-6364 DOI: 10.1039/C3TB21104E.
37. Henig, J.; Tóth, É.; Engelmann, J.; Gottschalk, S.; Mayer, H. A. Macrocyclic Gd3+ Chelates Attached to a Silsesquioxane Core as Potential Magnetic Resonance Imaging Contrast Agents: Synthesis, Physicochemical Characterization, and Stability Studies. *Inorg. Chem.* **2010,** 49 (13), 6124-6138 DOI: 10.1021/ic1007395.
38. Alam, M. M.; Bolze, F.; Daniel, C.; Flamigni, L.; Gourlaouen, C.; Heitz, V.; Jenni, S.; Schmitt, J.; Sour, A.; Ventura, B. π-Extended diketopyrrolopyrrole–porphyrin arrays: one- and

two-photon photophysical investigations and theoretical studies. *Phys. Chem. Chem. Phys.* **2016,** 18 (31), 21954-21965 DOI: 10.1039/C6CP01844K.
39. Ogunsipe, A.; Chen, J.-Y.; Nyokong, T. Photophysical and photochemical studies of zinc(ii) phthalocyanine derivatives—effects of substituents and solvents. *New J. Chem.* **2004,** 28 (7), 822-827 DOI: 10.1039/B315319C.
40. Seotsanyana-Mokhosi, I.; Kuznetsova, N.; Nyokong, T. Photochemical studies of tetra-2,3-pyridinoporphyrazines. *J. Photochem. Photobiol., A* **2001,** 140 (3), 215-222 DOI: https://doi.org/10.1016/S1010-6030(01)00427-0.
41. Nicoud, J.-F.; Bolze, F.; Sun, X.-H.; Hayek, A.; Baldeck, P. Boron-Containing Two-Photon-Absorbing Chromophores. 3. One- and Two-Photon Photophysical Properties of p-Carborane-Containing Fluorescent Bioprobes. *Inorg. Chem.* **2011,** 50 (10), 4272-4278 DOI: 10.1021/ic102043v.
42. Makarov, N. S.; Drobizhev, M.; Rebane, A. Two-photon absorption standards in the 550–1600 nm excitation wavelength range. *Opt. Express* **2008,** 16 (6), 4029-4047 DOI: 10.1364/OE.16.004029.
43. Xu, C.; Webb, W. W. Measurement of two-photon excitation cross sections of molecular fluorophores with data from 690 to 1050 nm. *J. Opt. Soc. Am. B* **1996,** 13 (3), 481-491 DOI: 10.1364/JOSAB.13.000481.
44. Powell, D. H.; Dhubhghaill, O. M. N.; Pubanz, D.; Helm, L.; Lebedev, Y. S.; Schlaepfer, W.; Merbach, A. E. Structural and Dynamic Parameters Obtained from 17O NMR, EPR, and NMRD Studies of Monomeric and Dimeric Gd3+ Complexes of Interest in Magnetic Resonance Imaging: An Integrated and Theoretically Self-Consistent Approach1. *J. Am. Chem. Soc.* **1996,** 118 (39), 9333-9346 DOI: 10.1021/ja961743g.

Table of Content graphic

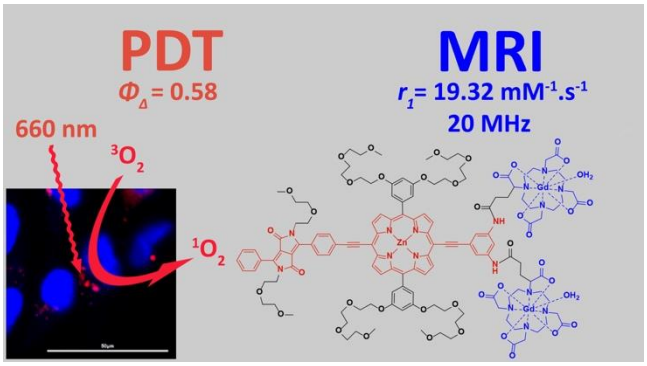

Synopsis

A porphyrin-based photosensitizer (PS) connected to two Gd(III) complexes has shown promising properties as a theranostic agent for combined photodynamic therapy (PDT) and magnetic resonance imaging (MRI). The conjugate has a high relaxivity for MRI applications, absorbs strongly at 670 nm and generates singlet oxygen upon irradiation. Moreover, the π-extended porphyrin core gives the molecule a two-photon absorption capacity in the near infrared. Preliminary PDT experiments have shown strong photoinduced toxicity on HeLa cells.